

Effects of nonstandard neutrino interactions at PINGU

Tommy Ohlsson,^{1,*} He Zhang,^{2,†} and Shun Zhou^{1,‡}

¹*Department of Theoretical Physics,
School of Engineering Sciences, KTH Royal Institute of Technology,
AlbaNova University Center, 106 91 Stockholm, Sweden*

²*Max-Planck-Institut für Kernphysik,
Saupfercheckweg 1, 69117 Heidelberg, Germany*

Abstract

Neutrino oscillation experiments in the past decades have greatly improved our knowledge on neutrinos by measuring the fundamental neutrino parameters. The ongoing and upcoming neutrino oscillation experiments are intended to pin down the neutrino mass hierarchy and to discover the leptonic CP violation. By means of neutrino oscillograms, we analyze the impact of non-standard neutrino interactions on neutrino oscillations in the Earth matter. The standard neutrino oscillation probabilities may be significantly changed by non-standard interaction parameters, and in particular, the CP-violating effects in the energy range $E = 1 \sim 20$ GeV are greatly enhanced. In addition, the event rates of muon neutrinos in the proposed huge atmospheric neutrino experiment, PINGU at the South Pole, have been estimated in the presence of non-standard neutrino interactions. It has been found that the PINGU experiment has very good sensitivities to the non-standard neutrino interaction parameters.

PACS numbers: 13.15.+g, 12.60.-i, 14.60.Pq

*Electronic address: tohlsson@kth.se

†Electronic address: he.zhang@mpi-hd.mpg.de

‡Electronic address: shunzhou@kth.se

I. INTRODUCTION

Today, the phenomenon of neutrino oscillations is considered to be the standard and leading order mechanism for neutrino flavor transitions, providing strong evidence that neutrinos are massive and lepton flavors are mixed, which leads to physics beyond the Standard Model (SM) of particle physics [1]. However, although it is widely accepted in the particle physics community that this phenomenon stems from a non-trivial structure of leptonic flavor mixing, the so-called non-standard neutrino interactions (NSIs), which are considered to be sub-leading order effects to standard neutrino oscillations, may still affect neutrino flavor transitions in a significant way [2]. The concept of NSIs is presently the most studied description for effects beyond the standard paradigm of neutrino oscillations. In fact, dimension-six and higher-order operators exist in various theoretical extensions of the SM, which include e.g. seesaw models, R -parity violating supersymmetric models, left-right symmetric models, grand unification theories, and extra dimensions. Basically, all modern extensions could give rise to NSIs. Therefore, the investigation of NSIs could reveal additional new physics behind neutrino flavor transitions. In addition, it plays an important complementary role to direct searches of physics beyond the SM at colliders such as the LHC.

For example, NSI effects have previously been studied for the accelerator-based neutrino oscillation experiments MINOS and OPERA [3, 4], atmospheric neutrino experiments [5–7], reactor neutrino experiments [8–10], and a future neutrino factory [11–15]. In this work, we investigate neutrino flavor transition probabilities based on standard neutrino oscillations and NSIs as sub-leading effects. Note that we only consider so-called propagation (or matter) NSIs, which are parameterized by different NSI parameters, and not source and detector NSIs. Especially, we derive oscillation probabilities for the $\nu_e \rightarrow \nu_\mu$ and $\nu_\mu \rightarrow \nu_\mu$ channels that are important for atmospheric neutrino oscillations, and study the impact of various NSI parameters on these probabilities, in both cases of the normal neutrino mass hierarchy (NH) and inverted neutrino mass hierarchy (IH). In addition, we estimate the number of atmospheric neutrino events in the future PINGU experiment at the South Pole, which has been recently shown to have great potential for determining the neutrino mass hierarchy [16–19]. Very good sensitivities to the NSI parameters are expected at this experiment.

The remaining part of our paper is organized as follows. In Sec. II, we will review the formalism of three-flavor neutrino oscillations in the presence of standard and non-standard matter effects, and present the parameter mappings between the leptonic mixing matrix in vacuum and that in matter. The analytical approximate formulas of oscillation probabilities are derived for the appearance channel $\nu_e \rightarrow \nu_\mu$ and disappearance channel $\nu_\mu \rightarrow \nu_\mu$. Sec. III is devoted to numerical analyses of the NSI effects on the neutrino oscillation probabilities with and without intrinsic CP violation. Using neutrino oscillograms, we further point out the important regions in the plane of zenith angles and neutrino energies, where the NSI effects are most significant. Taking into account the NSIs, we estimate the event rate of atmospheric muon neutrinos at the PINGU detector in Sec. IV. It turns out that the PINGU has very good sensitivities to the NSI parameters. Finally, we conclude in Sec. V.

II. NEUTRINO OSCILLATIONS WITH NSI

In general, NSIs can be present for neutrino production, propagation, and detection. We will concentrate on the non-standard matter effects for neutrino propagation, which should be relevant for atmospheric and long-baseline neutrino oscillation experiments in particular. In this section, we recall the general formulation of three-flavor neutrino oscillations in the presence of standard and non-standard matter effects. In this case, neutrino flavor transitions are determined by the effective Hamiltonian

$$\mathcal{H}(x) = \mathcal{H}_0 + \mathcal{H}_m(x) + \mathcal{H}_{\text{NSI}}(x) , \quad (1)$$

where the vacuum Hamiltonian is given by

$$\mathcal{H}_0 = \frac{1}{2E} U \begin{pmatrix} 0 & 0 & 0 \\ 0 & \Delta m_{21}^2 & 0 \\ 0 & 0 & \Delta m_{31}^2 \end{pmatrix} U^\dagger , \quad (2)$$

the standard matter potential is

$$\mathcal{H}_m(x) = V_{\text{CC}} \begin{pmatrix} 1 & 0 & 0 \\ 0 & 0 & 0 \\ 0 & 0 & 0 \end{pmatrix} , \quad (3)$$

with $V_{\text{CC}} = \sqrt{2}G_{\text{F}}N_e(x)$, and the non-standard matter potential is parametrized by

$$\mathcal{H}_{\text{NSI}}(x) = V_{\text{CC}} \begin{pmatrix} \varepsilon_{ee} & \varepsilon_{e\mu} & \varepsilon_{e\tau} \\ \varepsilon_{e\mu}^* & \varepsilon_{\mu\mu} & \varepsilon_{\mu\tau} \\ \varepsilon_{e\tau}^* & \varepsilon_{\mu\tau}^* & \varepsilon_{\tau\tau} \end{pmatrix} , \quad (4)$$

where $\varepsilon_{\alpha\beta}$ are real (for $\alpha = \beta$) or complex (for $\alpha \neq \beta$) constants, i.e., the so-called NSI parameters. Note that G_{F} is the Fermi constant and $N_e(x)$ is the electron number density in matter.

The exact oscillation probability is given by $P_{\alpha\beta} = |S_{\beta\alpha}(x, x_0)|^2$, where $S_{\beta\alpha}(x, x_0)$ is the evolution matrix satisfying the Schrödinger-like equation,

$$i \frac{d}{dx} |\nu(x)\rangle = \mathcal{H}(x) |\nu(x)\rangle , \quad (5)$$

and can be obtained by solving the above equation as

$$S(x, x_0) = \exp \left[-i \int_{x_0}^x \mathcal{H}(x') dx' \right] . \quad (6)$$

Since the standard matter potential \mathcal{H}_m is invariant under any rotation in the 2-3 plane, it is sometimes convenient to work in a new flavor basis $(\nu_e, \tilde{\nu}_2, \tilde{\nu}_3)^T = U_{23}(\nu_e, \nu_\mu, \nu_\tau)^T$ with $U_{23} \equiv O_{23}I_\delta$. Note that the leptonic mixing matrix can be parametrized as $U =$

$O_{23}I_\delta O_{13}I_\delta^\dagger O_{12}$, where O_{ij} denotes the rotation in the i - j plane with a rotation angle θ_{ij} and $I_\delta \equiv \text{diag}(1, 1, e^{i\delta})$ with δ being the leptonic Dirac CP-violating phase. If neutrinos are Majorana particles, there will be two additional CP-violating phases in U . However, these two leptonic Majorana CP-violating phases are irrelevant for neutrino oscillations both in vacuum and in matter.

Now, in this basis, the standard Hamiltonian can be written as

$$\tilde{\mathcal{H}}_{\text{SD}}(x) = \frac{1}{2E} O_{13} O_{12} \begin{pmatrix} 0 & 0 & 0 \\ 0 & \Delta m_{21}^2 & 0 \\ 0 & 0 & \Delta m_{31}^2 \end{pmatrix} O_{12}^T O_{13}^T + \mathcal{H}_m(x), \quad (7)$$

where $\tilde{\mathcal{H}}_{\text{SD}}(x) = U_{23}^\dagger \mathcal{H}_{\text{SD}}(x) U_{23}$ with $\mathcal{H}_{\text{SD}}(x) = \mathcal{H}_0 + \mathcal{H}_m(x)$, while the non-standard matter potential turns out to be

$$\tilde{\mathcal{H}}_{\text{NSI}}(x) = V_{\text{CC}} \begin{pmatrix} \varepsilon_{ee} & \tilde{\varepsilon}_{e\mu} & \tilde{\varepsilon}_{e\tau} \\ \tilde{\varepsilon}_{e\mu}^* & \tilde{\varepsilon}_{\mu\mu} & \tilde{\varepsilon}_{\mu\tau} \\ \tilde{\varepsilon}_{e\tau}^* & \tilde{\varepsilon}_{\mu\tau}^* & \tilde{\varepsilon}_{\tau\tau} \end{pmatrix}, \quad (8)$$

with the modified NSI parameters

$$\begin{aligned} \tilde{\varepsilon}_{e\mu} &= \varepsilon_{e\mu} c_{23} - \varepsilon_{e\tau} s_{23}, \\ \tilde{\varepsilon}_{e\tau} &= (\varepsilon_{e\mu} s_{23} + \varepsilon_{e\tau} c_{23}) e^{i\delta}, \\ \tilde{\varepsilon}_{\mu\mu} &= (\varepsilon_{\mu\mu} c_{23}^2 + \varepsilon_{\tau\tau} s_{23}^2) - 2s_{23} c_{23} \text{Re}[\varepsilon_{\mu\tau}], \\ \tilde{\varepsilon}_{\tau\tau} &= (\varepsilon_{\mu\mu} s_{23}^2 + \varepsilon_{\tau\tau} c_{23}^2) + 2s_{23} c_{23} \text{Re}[\varepsilon_{\mu\tau}], \\ \tilde{\varepsilon}_{\mu\tau} &= [(\varepsilon_{\mu\tau} c_{23}^2 - \varepsilon_{\mu\tau}^* s_{23}^2) + (\varepsilon_{\mu\mu} - \varepsilon_{\tau\tau}) s_{23} c_{23}] e^{i\delta}. \end{aligned} \quad (9)$$

Hence, in this basis, the effective Hamiltonian is

$$\tilde{\mathcal{H}}(x) = \Delta_{31} \left[\begin{pmatrix} s_{12}^2 c_{13}^2 \alpha + s_{13}^2 & s_{12} c_{12} c_{13} \alpha & s_{13} c_{13} (1 - s_{12}^2 \alpha) \\ s_{12} c_{12} c_{13} \alpha & c_{12}^2 \alpha & -s_{12} c_{12} s_{13} \alpha \\ s_{13} c_{13} (1 - s_{12}^2 \alpha) & -s_{12} c_{12} s_{13} \alpha & s_{12}^2 s_{13}^2 \alpha + c_{13}^2 \end{pmatrix} + A \begin{pmatrix} 1 + \varepsilon_{ee} & \tilde{\varepsilon}_{e\mu} & \tilde{\varepsilon}_{e\tau} \\ \tilde{\varepsilon}_{e\mu}^* & \tilde{\varepsilon}_{\mu\mu} & \tilde{\varepsilon}_{\mu\tau} \\ \tilde{\varepsilon}_{e\tau}^* & \tilde{\varepsilon}_{\mu\tau}^* & \tilde{\varepsilon}_{\tau\tau} \end{pmatrix} \right],$$

where $\Delta_{31} \equiv \Delta m_{31}^2 / (2E)$, $\alpha \equiv \Delta m_{21}^2 / \Delta m_{31}^2$ and $A \equiv V_{\text{CC}} / \Delta_{31}$. Additionally, note that $s_{ij} \equiv \sin \theta_{ij}$ and $\cos \theta_{ij} \equiv c_{ij}$ have been defined. The evolution matrix $\tilde{S}(x, x_0)$ in this basis is related to $S(x, x_0)$ in the flavor basis via the unitary transformation $S(x, x_0) = U_{23} \tilde{S}(x, x_0) U_{23}^\dagger$. The oscillation probabilities of antineutrinos can be obtained through the replacements $A \rightarrow -A$ and $\delta \rightarrow -\delta$.

A. Parameter Mappings

Now, following Refs. [20] and [21], we use a perturbation method to derive the effective neutrino masses \tilde{m}_i^2 and leptonic mixing matrix U^m in matter. Note that current neutrino oscillation data indicate $\alpha \sim \sqrt{2} s_{13}^2 \approx 0.03$. Therefore, we keep the terms of the same order

α and s_{13}^2 , and ignore all other higher-order contributions, such as αs_{13} , α^2 , and αs_{13}^2 . Thus, we write $\tilde{\mathcal{H}} = \mathcal{M} \cdot \Delta_{31}$ and introduce $\mathcal{M} \equiv \mathcal{M}^{(0)} + \mathcal{M}^{(1)}$:

$$\mathcal{M}^{(0)} = \begin{pmatrix} s_{13}^2 + A & 0 & s_{13}c_{13} \\ 0 & 0 & 0 \\ s_{13}c_{13} & 0 & c_{13}^2 \end{pmatrix}, \quad (10)$$

$$\mathcal{M}^{(1)} = \begin{pmatrix} s_{12}^2\alpha + A\varepsilon_{ee} & s_{12}c_{12}\alpha + A\tilde{\varepsilon}_{e\mu} & A\tilde{\varepsilon}_{e\tau} \\ s_{12}c_{12}\alpha + A\tilde{\varepsilon}_{e\mu}^* & c_{12}^2\alpha + A\tilde{\varepsilon}_{\mu\mu} & A\tilde{\varepsilon}_{\mu\tau} \\ A\tilde{\varepsilon}_{e\tau}^* & A\tilde{\varepsilon}_{\mu\tau}^* & A\tilde{\varepsilon}_{\tau\tau} \end{pmatrix}, \quad (11)$$

where $\mathcal{M}^{(0)}$ corresponds exactly to the standard Hamiltonian $\tilde{\mathcal{H}}_{\text{SD}}$ in the two-flavor limit with $\alpha = 0$, while $\mathcal{M}^{(1)}$ incorporates the corrections from α and the NSI parameters. Obviously, $\mathcal{M}^{(0)}$ can be diagonalized by a rotation in the 1-3 plane, i.e.,

$$U^{(0)} = \begin{pmatrix} \cos \hat{\theta}_{13} & 0 & \sin \hat{\theta}_{13} \\ 0 & 1 & 0 \\ -\sin \hat{\theta}_{13} & 0 & \cos \hat{\theta}_{13} \end{pmatrix} \quad (12)$$

with the effective mixing angle $\hat{\theta}_{13}$ given by

$$\tan 2\hat{\theta}_{13} = \frac{\sin 2\theta_{13}}{\cos 2\theta_{13} - A}. \quad (13)$$

In the following, we choose $\hat{\theta}_{13}$ to be defined in the first quadrant¹. Namely, $\hat{\theta}_{13} \in [0, \pi/4]$ for $A < \cos 2\theta_{13}$ and $\hat{\theta}_{13} \in [\pi/4, \pi/2]$ for $A > \cos 2\theta_{13}$. Therefore, we obtain [21]

$$\sin^2 \hat{\theta}_{13} = \frac{\hat{C} - \cos 2\theta_{13} + A}{2\hat{C}}, \quad \cos^2 \hat{\theta}_{13} = \frac{\hat{C} + \cos 2\theta_{13} - A}{2\hat{C}}, \quad (14)$$

with $\hat{C} \equiv \sqrt{(\cos 2\theta_{13} - A)^2 + \sin^2 2\theta_{13}}$. Two other useful relations can readily be derived from Eq. (14)

$$\sin 2\hat{\theta}_{13} = \frac{\sin 2\theta_{13}}{\hat{C}}, \quad \cos 2\hat{\theta}_{13} = \frac{\cos 2\theta_{13} - A}{\hat{C}}, \quad (15)$$

implying $\sin \hat{\theta}_{13} = \sin \theta_{13}/(1 - A)$ at the leading order of $\sin \theta_{13}$. In the limit of $\alpha = 0$ and in the absence of NSIs, $\hat{\theta}_{13}$ is just the effective mixing angle in matter.

Furthermore, the eigenvalues to zeroth order are given by

$$\begin{aligned} \lambda_1^{(0)} &= \frac{1}{2} \left(1 + A - \hat{C} \right), \\ \lambda_2^{(0)} &= 0, \\ \lambda_3^{(0)} &= \frac{1}{2} \left(1 + A + \hat{C} \right), \end{aligned} \quad (16)$$

¹ Note that it is also possible to define $\hat{\theta}_{13}$ to be in $[0, \pi/4]$ by properly arranging the eigenvalues and the corresponding eigenvectors, as shown in Ref. [22].

and the eigenvalues to first order are $\lambda_i^{(1)} = \tilde{\mathcal{M}}_{ii}^{(1)}$ with $\tilde{\mathcal{M}}^{(1)} = U^{(0)\dagger} \mathcal{M}^{(1)} U^{(0)}$. It is straightforward to show

$$\begin{aligned}\lambda_1^{(1)} &= \alpha \cos^2 \hat{\theta}_{13} s_{12}^2 + A \left[\cos^2 \hat{\theta}_{13} \varepsilon_{ee} - \sin 2\hat{\theta}_{13} \text{Re}(\tilde{\varepsilon}_{e\tau}) + \sin^2 \hat{\theta}_{13} \tilde{\varepsilon}_{\tau\tau} \right], \\ \lambda_2^{(1)} &= \alpha c_{12}^2 + A \tilde{\varepsilon}_{\mu\mu}, \\ \lambda_3^{(1)} &= \alpha \sin^2 \hat{\theta}_{13} s_{12}^2 + A \left[\sin^2 \hat{\theta}_{13} \varepsilon_{ee} + \sin 2\hat{\theta}_{13} \text{Re}(\tilde{\varepsilon}_{e\tau}) + \cos^2 \hat{\theta}_{13} \tilde{\varepsilon}_{\tau\tau} \right].\end{aligned}\quad (17)$$

The corrections to the eigenvectors are given by

$$U_i^{(1)} = \sum_{j \neq i} \frac{\tilde{\mathcal{M}}_{ji}^{(1)}}{\lambda_i^{(0)} - \lambda_j^{(0)}} U_j^{(0)}, \quad (18)$$

where $U_i^{(1)}$ and $U_j^{(0)}$ stand for the column vectors of the matrices $U^{(1)}$ and $U^{(0)}$, respectively. The effective neutrino masses in matter are determined by $\tilde{m}_i^2 = m_1^2 + \Delta m_{31}^2 [\lambda_i^{(0)} + \lambda_i^{(1)}]$, while the effective leptonic mixing matrix is $U^m = U_{23} [U^{(0)} + U^{(1)}]$. In the absence of NSIs, there are two resonances, i.e., $A = \alpha$ and $A = \cos 2\theta_{13}$. For neutrino energies $E > 1$ GeV and matter densities $\rho = 3$ g/cm³ in the Earth crust, we have $A > \alpha$, so only the resonance $A = \cos 2\theta_{13}$ is relevant [22]. Now, after some lengthy computations, we find that

$$\begin{aligned}U_{e3}^m &= \sin \hat{\theta}_{13} + \frac{\cos \hat{\theta}_{13}}{2\hat{C}} \left\{ \sin 2\hat{\theta}_{13} [\alpha s_{12}^2 + A(\varepsilon_{ee} - \tilde{\varepsilon}_{\tau\tau})] + 2A [\cos 2\hat{\theta}_{13} \text{Re}(\tilde{\varepsilon}_{e\tau}) + i\text{Im}(\tilde{\varepsilon}_{e\tau})] \right\}, \\ U_{e2}^m &= -\frac{c_{13}}{2A} \alpha \sin 2\theta_{12} - \tilde{\varepsilon}_{e\mu} + \frac{\tan \theta_{13}}{A} \tilde{\varepsilon}_{\mu\tau}^*, \\ U_{\mu 3}^m &= s_{23} \cos \hat{\theta}_{13} e^{i\delta} \left\{ 1 - \frac{A \tan \hat{\theta}_{13}}{\hat{C}} [\cos 2\hat{\theta}_{13} \text{Re}(\tilde{\varepsilon}_{e\tau}) + i\text{Im}(\tilde{\varepsilon}_{e\tau})] \right\} + \frac{\alpha c_{23} \sin 2\theta_{12} \sin \hat{\theta}_{13}}{1 + A + \hat{C}},\end{aligned}\quad (19)$$

which reproduce the well-known results in the limit of vanishing NSI parameters [22, 23]. Our results in Eq. (19) differ from those in Ref. [23] by including higher-order corrections from α and s_{13} . The parameter mapping is not valid in the resonance region, where the perturbation theory breaks down. Furthermore, the mixing matrix elements in matter could be divergent, so we will calculate the oscillation probabilities that should be well-defined in general, and particularly in the resonance region. As pointed out in Ref. [22], the mixing angle θ_{12} can be arbitrary in the limit of $\alpha = 0$ and in the absence of the NSIs, so the mapping for U_{e2}^m in Eq. (19) cannot be taken seriously. For neutrino energies $E > 1$ GeV, only the effective mixing angle $\tilde{\theta}_{13}$, which is determined by U_{e3}^m in the standard parametrization [1], is crucially important for neutrino oscillations in the Earth matter. Note that the true effective mixing angle $\tilde{\theta}_{13}$ differs from $\hat{\theta}_{13}$ in the contributions from α and the NSI parameters.

B. Oscillation Probabilities

In practice, the oscillation probabilities can be computed using perturbation theory based on small quantities, e.g., the smallest mixing angle θ_{13} , the ratio of the two mass-squared

differences α , and the NSI parameters $\varepsilon_{\alpha\beta}$. Following Ref. [21], one can explicitly decompose the effective Hamiltonian as $\mathcal{H}(x) = \mathcal{H}'_0(x) + \mathcal{H}_1(x)$, where $\mathcal{H}'_0(x)$ is the zeroth order in the small parameters and $\mathcal{H}_1(x)$ includes the higher-order contributions. Then, to first order, the evolution matrix is approximately given by

$$S(x, x_0) \simeq S_0(x, x_0) - iS_0(x, x_0) \int_{x_0}^x [S_0(x', x_0)^{-1} \mathcal{H}_1(x') S_0(x', x_0)] dx', \quad (20)$$

where the zeroth-order evolution matrix $S_0(x, x_0)$ is determined by $\mathcal{H}'_0(x)$. For constant matter density, the oscillation probability for the $\nu_e \rightarrow \nu_\mu$ channel is found to be [8, 12, 24]

$$\begin{aligned} P_{e\mu}^{\text{NSI}} \simeq P_{e\mu}^{\text{SD}} &- 4\tilde{s}_{13}s_{23}c_{23} (|\varepsilon_{e\mu}|c_{23}c_\chi - |\varepsilon_{e\tau}|s_{23}c_\omega) \left[\sin^2 \frac{A\Delta}{2} - \sin^2 \frac{\Delta}{2} + \sin^2 \frac{(1-A)\Delta}{2} \right] \\ &+ 8\tilde{s}_{13}s_{23}^2 [|\varepsilon_{e\mu}|s_{23}c_\chi + |\varepsilon_{e\tau}|c_{23}c_\omega] \frac{A}{1-A} \sin^2 \frac{(1-A)\Delta}{2} \\ &+ 8\tilde{s}_{13}s_{23}c_{23} (|\varepsilon_{e\mu}|c_{23}s_\chi - |\varepsilon_{e\tau}|s_{23}s_\omega) \sin \frac{A\Delta}{2} \sin \frac{\Delta}{2} \sin \frac{(1-A)\Delta}{2}, \end{aligned} \quad (21)$$

where $\Delta \equiv \Delta_{31}L$ denotes the oscillation phase in vacuum, and $\tilde{s}_{13} = s_{13}/(1-A)$ is just $\sin \tilde{\theta}_{13}$ in the leading order. In addition, we have defined $\varepsilon_{\alpha\beta} = |\varepsilon_{\alpha\beta}|e^{i\phi_{\alpha\beta}}$ (for $\alpha\beta = e\mu, e\tau$), $\chi = \phi_{e\mu} + \delta$, and $\omega = \phi_{e\tau} + \delta$. Note that we have neglected the terms proportional to $\alpha \varepsilon_{\alpha\beta}$, and $P_{e\mu}^{\text{SD}}$ stands for the transition probability without the NSIs, i.e., $P_{e\mu}^{\text{SD}} \simeq 4\tilde{s}_{13}^2s_{23}^2 \sin^2 \frac{(1-A)\Delta}{2}$. The approximate formulas of neutrino oscillation probabilities to the second order of α and s_{13} can be found in Ref. [21]. At leading order, only the NSI parameters $\varepsilon_{e\mu}$ and $\varepsilon_{e\tau}$ appear in the transition probability $P_{e\mu}^{\text{NSI}}$ [8, 12]. Hence, we will concentrate on these two parameters in following numerical analysis. Furthermore, the CP-violating terms in the last line of Eq. (21) related to NSI parameters are not suppressed by the ratio of two mass-squared differences α , compared to the standard case. Thus, even when the standard CP violation is not visible in an experimental setup, one may expect observable CP-violating effects stemming from the catalysis of NSIs.

Next, for the $\nu_\mu \rightarrow \nu_\mu$ channel, we have [8, 12, 24]

$$\begin{aligned} P_{\mu\mu}^{\text{NSI}} \simeq P_{\mu\mu}^{\text{SD}} &- |\varepsilon_{\mu\tau}|c_{\phi_{\mu\tau}} \left(s_{2\times 23}^3 A\Delta \sin \Delta + 4s_{2\times 23}c_{2\times 23}^2 A \sin^2 \frac{\Delta}{2} \right) \\ &+ (|\varepsilon_{\mu\mu}| - |\varepsilon_{\tau\tau}|)s_{2\times 23}^2c_{2\times 23} \left(\frac{A\Delta}{2} \sin \Delta - 2A \sin^2 \frac{\Delta}{2} \right), \end{aligned} \quad (22)$$

where $\varepsilon_{\mu\tau} \equiv |\varepsilon_{\mu\tau}|e^{i\phi_{\mu\tau}}$, $s_{2\times 23} \equiv \sin 2\theta_{23}$ and $c_{2\times 23} \equiv \cos 2\theta_{23}$ have been defined. Note that only the NSI parameters $\varepsilon_{\mu\mu}$, $\varepsilon_{\mu\tau}$, and $\varepsilon_{\tau\tau}$ appear in the survival probability $P_{\mu\mu}^{\text{NSI}}$ [8]. Since the current experimental bound on $\varepsilon_{\mu\mu}$ is very stringent, the dominant NSI effects should come from $\varepsilon_{\mu\tau}$ and $\varepsilon_{\tau\tau}$.

III. NUMERICAL ANALYSIS

In order to illustrate the NSI effects on neutrino propagation in the Earth, we calculate numerically the effective mixing angle $\tilde{\theta}_{13}$ and the oscillation probabilities. In our numerical

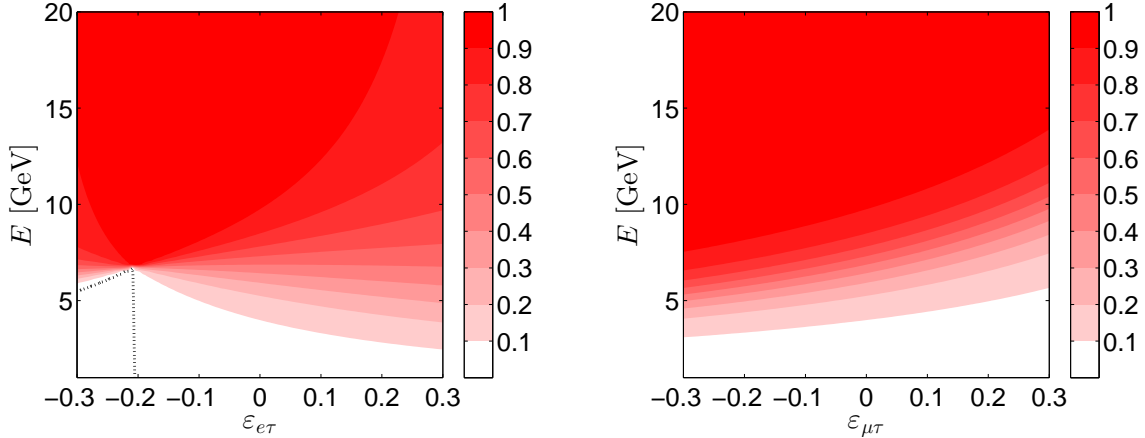


FIG. 1: Dependence of the effective mixing angle $\sin^2 \tilde{\theta}_{13}$ on the NSI parameters and neutrino energy, where a constant matter density profile $\rho = 4.5 \text{ g/cm}^3$ has been assumed (i.e., the Earth mantle density) and the dotted line corresponds to $\sin^2 \tilde{\theta}_{13} = \sin^2 \theta_{13}$. In addition, the best-fit values of neutrino parameters (i.e., $\sin^2 \theta_{12} = 0.30$, $\sin^2 \theta_{23} = 0.41$, $\sin^2 \theta_{13} = 0.023$, $\Delta m_{21}^2 = 7.50 \times 10^{-5} \text{ eV}^2$, and $\Delta m_{31}^2 = 2.47 \times 10^{-3} \text{ eV}^2$) from Ref. [29] have been used.

computations, we assume the Preliminary Reference Earth model of Earth's matter density [25], and express the baseline in terms of the zenith angle as $L = -2R \cos \theta_z$, where $R = 6371 \text{ km}$ is the Earth radius and $\theta_z = \pi - h$ with h being the nadir angle. Note that $-1 < \cos \theta_z < -0.84$ corresponds to the trajectories crossing both the mantle and core of the Earth, while $-0.84 < \cos \theta_z < 0$ to those crossing only the Earth mantle. On the other hand, there already exist restrictive experimental constraints on the NSI parameters in realistic models [26]. However, in Ref. [27], the model-independent upper bounds on the matter NSI parameters have been found to be much larger than the model-dependent ones:

$$\left(\begin{array}{ccc} |\varepsilon_{ee}| < 4.2 & |\varepsilon_{e\mu}| < 0.33 & |\varepsilon_{e\tau}| < 3.0 \\ & |\varepsilon_{\mu\mu}| < 0.068 & |\varepsilon_{\mu\tau}| < 0.33 \\ & & |\varepsilon_{\tau\tau}| < 21 \end{array} \right). \quad (23)$$

Therefore, in the following discussions, we just ignore $\varepsilon_{\mu\mu}$, which receives the most stringent constraint. For the other matter NSI parameters, we will take a conservative value $|\varepsilon_{\alpha\beta}| = 0.1$ for illustration ².

A. Effective Mixing Angle in Matter

First of all, it may be interesting to show how the standard and non-standard matter effects modify the effective neutrino mixing angles $\tilde{\theta}_{ij}$ in matter. As mentioned in the

² Recently, the MINOS experiment has constrained the NSI parameter to the range $-0.20 < \varepsilon_{\mu\tau} < 0.07$ at the 90% confidence level [28], in the framework of two-flavor neutrino oscillations.

previous section, we will focus on $\tilde{\theta}_{13}$, which is relevant for neutrino energies $E > 1$ GeV. To examine the dependence of $\tilde{\theta}_{13}$ on the NSI parameters, we consider two specific examples, where only one relevant NSI parameter is switched on in each case and all the CP-violating phases (i.e., δ and $\phi_{\alpha\beta}$) are set to zero:

- $\varepsilon_{e\tau} \neq 0$. With the help of Eqs. (9) and (19), we derive

$$\sin^2 \tilde{\theta}_{13} = \frac{\hat{C} - \cos 2\theta_{13} + A}{2\hat{C}} + \frac{\cos 2\theta_{13} - A}{\hat{C}^3} A \sin 2\theta_{13} c_{23} \varepsilon_{e\tau}, \quad (24)$$

where the small terms α_{s13} and $\varepsilon_{e\tau}^2$ have been neglected. It is worthwhile to mention that if the resonance condition $A = \cos 2\theta_{13}$ is satisfied, we have $\tilde{\theta}_{13} = \pi/4$, which is independent of the NSI parameter $\varepsilon_{e\tau}$ in the leading order approximation. This can be well understood in the framework of two-flavor neutrino oscillations in matter with NSIs [4, 30], where one observes that the off-diagonal term in \mathcal{H}_{NSI} cannot modify the resonance condition. The result in the case of $\varepsilon_{e\mu} \neq 0$ can be obtained by replacing $c_{23}\varepsilon_{e\tau}$ with $s_{23}\varepsilon_{e\mu}$ in Eq (24), and the difference between these two cases can be attributed to a non-maximal θ_{23} . In Fig. 1, we have calculated $\sin^2 \tilde{\theta}_{13}$ using the exact formulas of parameter mappings [23]. From the left panel, we can clearly observe that the resonance condition is essentially unchanged by $\varepsilon_{e\tau}$, and $\tilde{\theta}_{13} = \theta_{13}$ is achieved when the standard matter effects are cancelled by the NSI effects. However, the resonance is in fact shifted by higher-order corrections.

- $\varepsilon_{\mu\tau} \neq 0$. In a similar way, we obtain

$$\sin^2 \tilde{\theta}_{13} = \frac{\hat{C} - \cos 2\theta_{13} + A}{2\hat{C}} - \frac{\sin^2 2\theta_{13}}{2\hat{C}^3} A \sin 2\theta_{23} \varepsilon_{\mu\tau}, \quad (25)$$

where the small terms α_{s13} and $\varepsilon_{\mu\tau}^2$ have been omitted. It is now evident that the standard resonance condition $A = \cos 2\theta_{13}$ does not lead to $\sin^2 \tilde{\theta}_{13} = 1/2$. Namely, the resonance has been shifted by the NSI parameter, which has also been pointed out in Ref. [30] in the framework of two-neutrino oscillations. For a fixed value of $\tilde{\theta}_{13}$, if $\varepsilon_{\mu\tau}$ becomes larger, the neutrino energy has to increase in order to balance the negative contribution from $\varepsilon_{\mu\tau}$. In the right panel of Fig. 1, we have shown $\sin^2 \tilde{\theta}_{13}$ by using the exact mapping formulas. The main features can be well described by the approximate formula in Eq. (25). Note that, compared to $\varepsilon_{e\tau}$, the $\varepsilon_{\mu\tau}$ correction to $\tilde{\theta}_{13}$ is milder since it is further suppressed by $\sin 2\theta_{13}$. Similarly, one can also consider the impact of ε_{ee} , $\varepsilon_{\mu\mu}$, and $\varepsilon_{\tau\tau}$ on the effective mixing angles.

B. Neutrino Oscillograms: Standard Case

The matter effects on neutrino propagation in the Earth can be perfectly illustrated through the so-called neutrino oscillograms. In order to compare between standard and

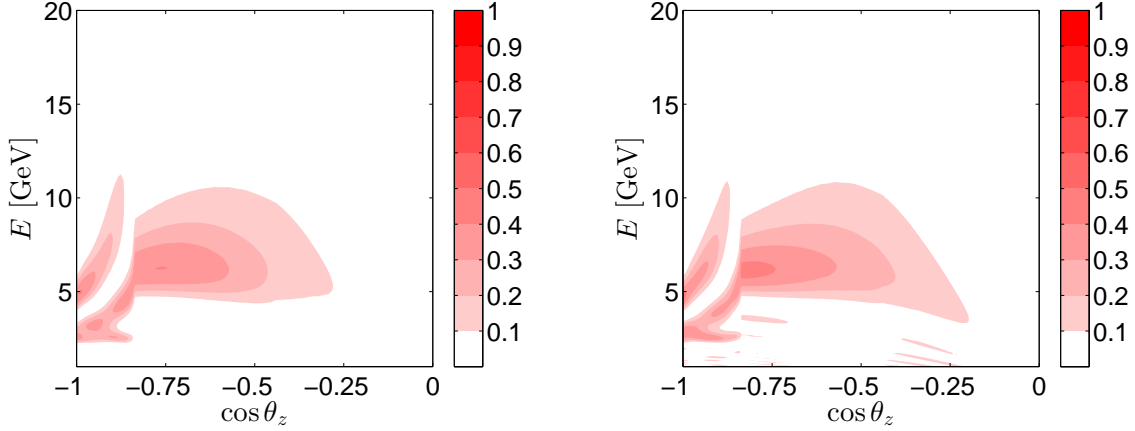


FIG. 2: Standard neutrino oscillograms without NSIs (i.e., $\varepsilon_{\alpha\beta} = 0$) in the appearance channel: $P_{e\mu}^{\text{SD}} = P(\nu_e \rightarrow \nu_\mu)$ for neutrino oscillations in the case of normal neutrino mass hierarchy (left panel) and $\bar{P}_{e\mu}^{\text{SD}} = P(\bar{\nu}_e \rightarrow \bar{\nu}_\mu)$ for antineutrino oscillations in the case of inverted neutrino mass hierarchy (right panel).

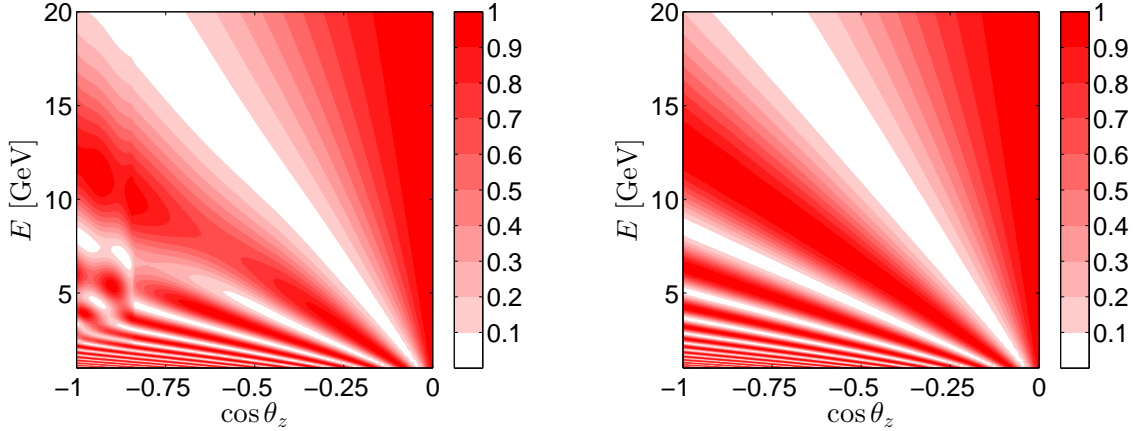


FIG. 3: Standard neutrino oscillograms without NSIs (i.e., $\varepsilon_{\alpha\beta} = 0$) in the disappearance channel: $P_{\mu\mu}^{\text{SD}} = P(\nu_\mu \rightarrow \nu_\mu)$ for neutrino oscillations in the case of normal neutrino mass hierarchy (left panel) and in the case of inverted neutrino mass hierarchy (right panel).

non-standard matter effects, we first briefly summarize the general features of the standard neutrino oscillograms, which have been systematically studied in Refs. [31, 32].

In Figs. 2 and 3, we have reproduced the neutrino oscillograms in the $\nu_e \rightarrow \nu_\mu$ and $\nu_\mu \rightarrow \nu_\mu$ channels, respectively. In our numerical calculations, the latest global-fit data on leptonic mixing angles (i.e., $\sin^2 \theta_{12} = 0.30$, $\sin^2 \theta_{23} = 0.41$, and $\sin^2 \theta_{13} = 0.023$) and the neutrino mass-squared differences (i.e., $\Delta m_{21}^2 = 7.50 \times 10^{-5} \text{ eV}^2$ and $|\Delta m_{31}^2| = 2.47 \times 10^{-3} \text{ eV}^2$) given in Ref. [29] have been used. Since the Dirac CP-violating phase has not been experimentally constrained, we simply take $\delta = 0$ in the calculations. Some general comments on the neutrino oscillograms are in order [31]:

- In the left panel of Fig. 2, the oscillation probability $P_{e\mu}^{\text{SD}} \equiv P(\nu_e \rightarrow \nu_\mu)$ is shown in the NH case. The resonance in the mantle appears around $\cos\theta_z^{\text{R}} \approx -0.75$ and $E_{\text{R}} \approx 6$ GeV, where the resonance energy E_{R} is essentially determined by $A = \cos 2\theta_{13}$ while the corresponding baseline L_{R} or the zenith angle θ_z^{R} by the requirement of maximal oscillation phase $\Delta = \pi$. Note that we can safely ignore the effects of Δm_{21}^2 for neutrino energies $E > 1$ GeV. The ridges in the core region are caused by the parametric resonances, receiving both contributions from the mantle and core oscillation phases [31]. Since the resonance takes place in the neutrino sector, the oscillation probability of $\bar{\nu}_e \rightarrow \bar{\nu}_\mu$ is suppressed by matter effects and the oscillogram is almost empty. In the right panel of Fig. 2, we have calculated the antineutrino oscillation probability $\bar{P}_{e\mu}^{\text{SD}} \equiv P(\bar{\nu}_e \rightarrow \bar{\nu}_\mu)$ in the IH case. Now that the resonances occur in this case and dominate the contributions to oscillation probabilities, the similarity between $P_{e\mu}^{\text{SD}}$ for NH and $\bar{P}_{e\mu}^{\text{SD}}$ for IH is evident. The oscillation probability $\bar{P}_{e\mu}^{\text{SD}}$ in the NH case is highly suppressed, as $P_{e\mu}^{\text{SD}}$ in the IH case.
- In Fig. 3, we have given the survival probabilities $P_{\mu\mu}^{\text{SD}} \equiv P(\nu_\mu \rightarrow \nu_\mu)$ for both NH (left panel) and IH (right panel). The probability $P_{\mu\mu}^{\text{SD}}$ receives the dominant contribution from the vacuum oscillation due to θ_{23} and Δm_{31}^2 , and is significantly affected by the 1-3 mixing through θ_{13} only in the resonance regions. In fact, the latter effect reduces $P_{\mu\mu}^{\text{SD}}$, as indicated in the left panel of Fig. 3. In the absence of resonance, as in the IH case, $P_{\mu\mu}^{\text{SD}}$ is basically given by the vacuum oscillation probability as shown in the right panel. The antineutrino survival probabilities $\bar{P}_{\mu\mu}^{\text{SD}} \equiv P(\bar{\nu}_\mu \rightarrow \bar{\nu}_\mu)$ in NH and IH cases are similar to $P_{\mu\mu}^{\text{SD}}$ in IH and NH cases, respectively.

The detailed study of the maxima and minima in neutrino oscillation probabilities and the general conditions for resonances in the two-flavor approximation can be found in Ref. [31], while those for the three-flavor oscillations in Ref. [32]. In our discussions, since the neutrino energies are always above 1 GeV, the three-flavor corrections should be negligible.

C. Neutrino Oscillograms: NSI Effects

Now we proceed to discuss the NSI effects on the standard neutrino oscillations in the Earth by using neutrino oscillograms. To quantify the NSI effects, we consider the difference between the standard (i.e., $\varepsilon_{\alpha\beta} = 0$) and non-standard (i.e., $\varepsilon_{\alpha\beta} \neq 0$) neutrino oscillograms, namely $\Delta P_{e\mu} = P_{e\mu}^{\text{NSI}} - P_{e\mu}^{\text{SD}}$ and $\Delta P_{\mu\mu} = P_{\mu\mu}^{\text{NSI}} - P_{\mu\mu}^{\text{SD}}$. In Fig. 4, we numerically calculate $\Delta P_{e\mu}$ and $\Delta P_{\mu\mu}$ in the NH case, and only one NSI parameter is switched on in each plot.

First, we consider the difference $\Delta P_{e\mu}$ in the appearance channel, for which the approximate formula in the case of constant matter density can be obtained from Eq. (21) and the numerical results are shown in the left column of Fig. 4. Two comments are in order: (1) The contributions from NSI parameters to $\Delta P_{e\mu}$ are proportional to s_{13} in the limit $A \rightarrow 1$, i.e., around the resonance. In the deep core, i.e., $\cos\theta_z < -0.84$, the parametric resonances dominate, so the NSI effects are not necessarily suppressed. (2) The difference

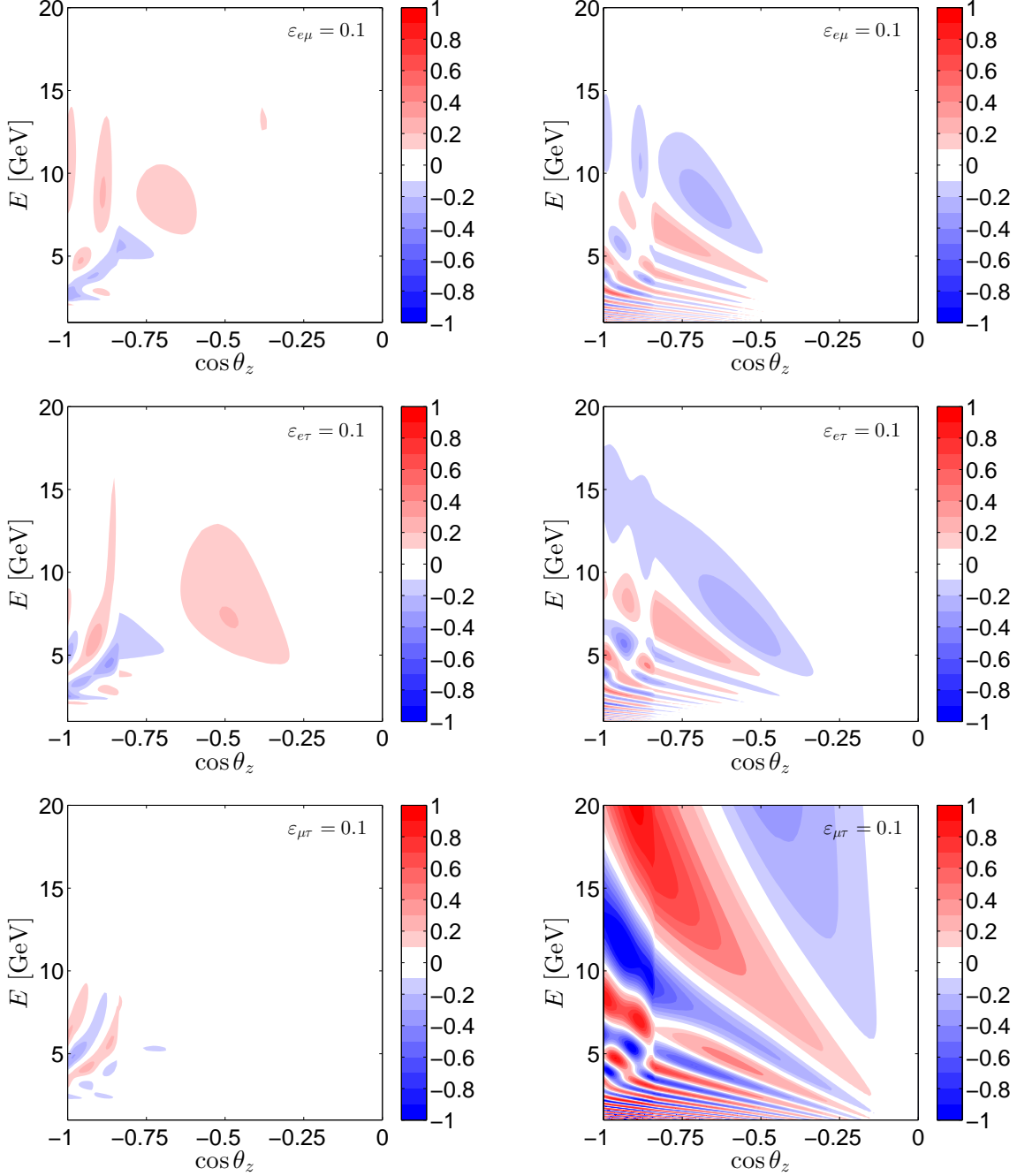


FIG. 4: Differences between the standard and non-standard neutrino oscillograms in the $\nu_e \rightarrow \nu_\mu$ channel $\Delta P_{e\mu} \equiv P_{e\mu}^{\text{NSI}} - P_{e\mu}^{\text{SD}}$ (left column) and in the $\nu_\mu \rightarrow \nu_\mu$ channel $\Delta P_{\mu\mu} \equiv P_{\mu\mu}^{\text{NSI}} - P_{\mu\mu}^{\text{SD}}$ (right column), where the normal neutrino mass hierarchy and $\delta = 0$ are assumed, and $\varepsilon_{e\mu} = 0.1$ (upper row), $\varepsilon_{e\tau} = 0.1$ (middle row), and $\varepsilon_{\mu\tau} = 0.1$ (lower row) are taken for illustration.

$\Delta P_{e\mu}$ is independent of $\varepsilon_{\mu\tau}$ in leading order. For this reason, as shown in the lower plot, $\Delta P_{e\mu}$ is vanishing everywhere except in the core, if only $\varepsilon_{\mu\tau} \neq 0$ is assumed. One common feature of all three plots is that significant NSI effects are lying in the core region, which is only accessible in the atmospheric neutrino experiments.

Second, we turn to the difference $\Delta P_{\mu\mu}$ in the disappearance channel, for which the approximate formula in the case of constant matter density can be obtained from Eq. (22) and the numerical results are shown in the right column of Fig. 4. As implied by Eq. (22), the effects induced by $\varepsilon_{e\mu}$ and $\varepsilon_{e\tau}$ can only arise from higher-order corrections of s_{13} and α , so they are insignificant as in the upper and middle plots. The most interesting observation is that $|\Delta P_{\mu\mu}| \simeq 1$ could be achieved, particularly in the core region. Switching off both $\varepsilon_{\mu\mu}$ and $\varepsilon_{\tau\tau}$ in Eq. (22), we have

$$\Delta P_{\mu\mu} \approx -|\varepsilon_{\mu\tau}| \sin 2\theta_{23} \left(A\Delta \sin^2 2\theta_{23} \sin \Delta + 4 \cos^2 2\theta_{23} \sin^2 \frac{\Delta}{2} \right), \quad (26)$$

where $\phi_{\mu\tau} = 0$ is assumed. Furthermore, note that the second term in the parentheses on the right-hand side of Eq. (26) is always positive, while the first term can be either positive or negative, depending on the oscillation phase Δ . If $\Delta = (2k + 1)\pi/2$ with k being an integer, the contribution from the second term is negligible, since $\cos^2 2\theta_{23} \approx 0.03$ for the best-fit value of $\theta_{23} = 40^\circ$. Therefore, $\Delta P_{\mu\mu} \propto \sin \Delta$ should show an oscillatory behavior, as given in the lower plot. It is worthwhile to note that $\Delta = (2k + 1)\pi/2$ corresponds to the oscillation minima of the standard survival probability $P_{\mu\mu}^{\text{SD}}$. For example, comparing the left plot of Fig. 3 with the lower plot in the right column of Fig. 4, one can observe the huge difference in the region along the diagonal line. If $\Delta = k\pi$ holds, the second term dominates over the first one, and $\Delta P_{\mu\mu}$ follow the same oscillatory structure as the leading vacuum oscillation term in $P_{\mu\mu}^{\text{SD}}$.

D. Non-Standard CP Violation

Finally, we show that the NSIs may lead to the enhancement of CP-violating effects in neutrino oscillations [33]. In Fig. 5, the probability differences $\Delta P_{e\mu}(\delta) \equiv P_{e\mu}^{\text{NSI}}(\delta) - P_{e\mu}^{\text{NSI}}(0)$ induced by the leptonic CP violating phase δ are calculated for $\delta = \pi/2$. To signify the CP-violating effects due to δ , we set all the NSI phase parameters to zero, i.e., $\phi_{\alpha\beta} = 0$. As mentioned before, the CP-violating effects in the standard case come from the interference between two different oscillation frequencies, and thus these effects are relatively small in both cases of NH and IH. However, the probability differences are enhanced greatly when the NSI parameters are switched on, in particular in the NH case.

The left and right plots in the first row correspond to $\Delta P_{e\mu}(\delta) = P_{e\mu}^{\text{SD}}(\delta) - P_{e\mu}^{\text{SD}}(0)$ in the NH and IH cases, respectively, since the NSI parameters are taken to be zero. One can observe that the impact of δ is insignificant. See Ref. [34] for more discussions about the CP-violating effects in the standard three-neutrino oscillations in matter. Even if the NSI parameters are nonzero, the CP-violating effects are negligible in the IH case, as shown in the middle and lower plots in the right column. This is because the transition probability $P_{e\mu}^{\text{NSI}}$ itself is suppressed rather than enhanced by matter effects. However, as in the NH case, $|\Delta P_{e\mu}(\delta)|$ for $\delta = \pi/2$ could be 12% in the mantle, while as large as 30% in the core, as illustrated in the middle and lower plots in the left column. At the same time, without the

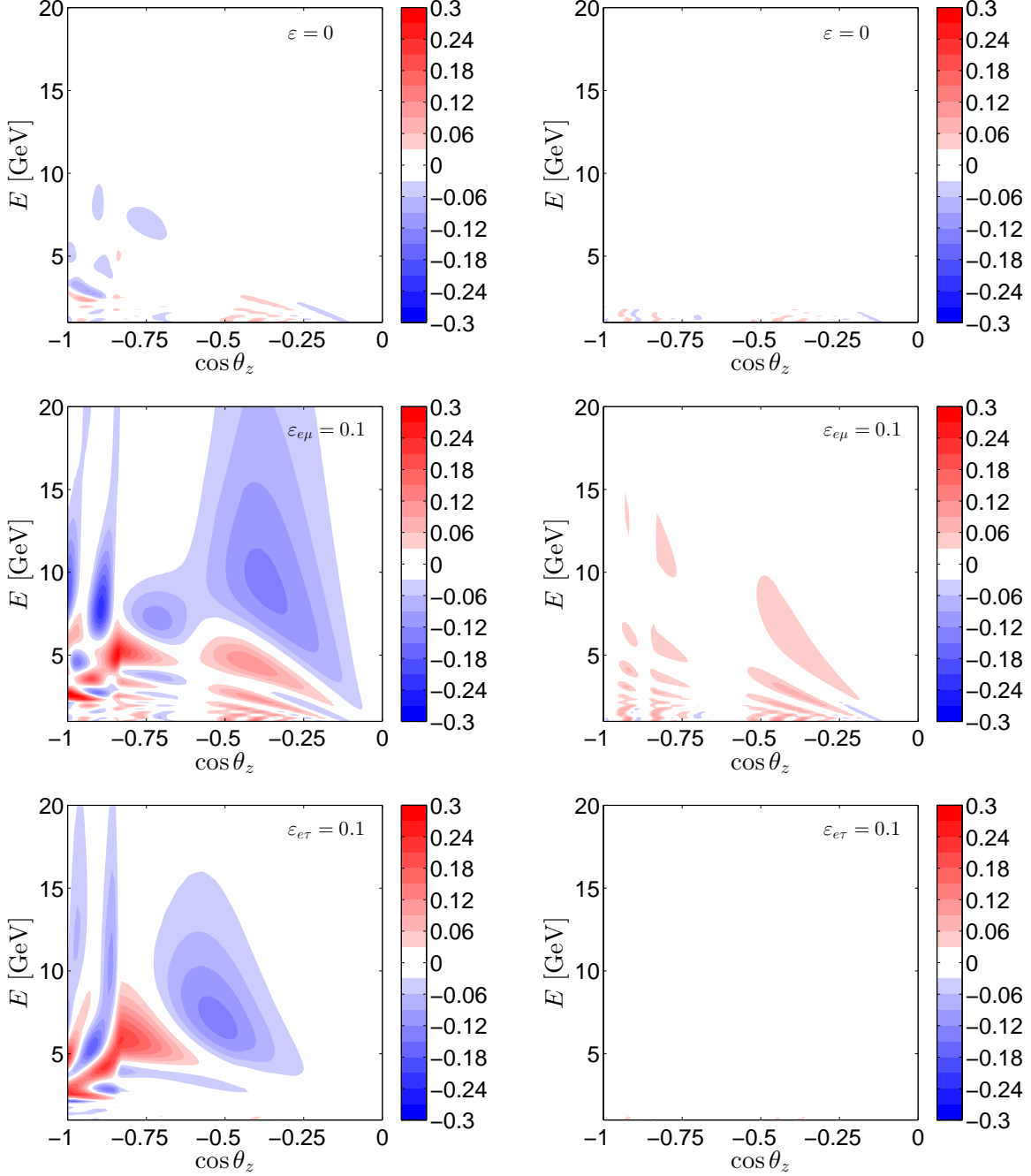


FIG. 5: Oscillograms for the probability differences $\Delta P_{e\mu}(\delta) = P_{e\mu}^{\text{NSI}}(\delta) - P_{e\mu}^{\text{NSI}}(0)$ with $\delta = \pi/2$ in the normal neutrino mass hierarchy case (left column) and in the inverted neutrino mass hierarchy case (right column). The two plots in the first row correspond to $\Delta P_{e\mu}(\delta)$ with vanishing NSI parameters, i.e., $\Delta P_{e\mu}(\delta) = P_{e\mu}^{\text{SD}}(\delta) - P_{e\mu}^{\text{SD}}(0)$ with $\delta = \pi/2$.

NSI effects, it is vanishingly small in both mantle and core regions. Therefore, the future long-baseline oscillation experiments, where neutrino beams traverse the Earth mantle, will have excellent sensitivities to NSI-enhanced CP-violating effects.

The remarkable difference between standard and non-standard CP-violating effects be-

comes clear, if we look at the last line of Eq. (21). More explicitly, $\Delta P_{e\mu}(\delta)$ is proportional to αs_{13} in the standard case, while to $|\varepsilon_{e\mu}|s_{13}$ or $|\varepsilon_{e\tau}|s_{13}$ in the non-standard case. For $\varepsilon_{\alpha\beta} = 0.1$ and $\alpha \approx 0.03$, the standard CP violation is suppressed by one order of magnitude.

IV. EVENT RATES AT PINGU

In previous sections, we have explored the general features of NSI effects on neutrino oscillations in the Earth matter at the level of oscillation probabilities, which should have important implications for atmospheric neutrino experiments. In order to study the NSI effects in a realistic experiment, we have to calculate the number of neutrino events in small bins of energies ΔE and zenith angles $\Delta \cos \theta_z$ for a terrestrial detector. To this end, we take a multi-megaton scale ice Cherenkov detector for example, such as the proposed PINGU detector at the South Pole [35]. The main idea of this proposal is to make the Deep Core of the IceCube detector denser to lower the energy threshold down to a few GeV, implying possible precision measurements of atmospheric neutrinos. Such an experimental setup would be rather interesting in view of its great physics potential for the determination of neutrino mass hierarchy, and the oscillation parameters [16–19]. We refer the readers to Ref. [35] for a detailed description of the PINGU experiment.

Atmospheric neutrinos interact with the nucleons via charged-current interactions in the detector and produce energetic charged leptons, which are radiating Cherenkov photons when propagating in ice. The Cherenkov photons will be captured by the dense strings of photomultipliers. The charged muons μ^\pm leave clear and long tracks in the detector, so the experimental resolution to the direction of muon neutrinos is much better than that of electron neutrinos. Now, we make a rough estimate of the distribution of ν_μ -like events collected by the PINGU detector for one year running. Explicitly, the number of ν_μ -like events in the i -th zenith-angle bin and j -th energy bin is given by

$$N_{ij} = 2\pi N_A T \int_{\cos \theta_z^i}^{\cos \theta_z^{i+1}} d \cos \theta_z \int_{E_j}^{E_{j+1}} dE \left[\left(\frac{d\Phi_{\nu_\mu}}{d \cos \theta_z dE} P_{\mu\mu}^{\text{NSI}} + \frac{d\Phi_{\nu_e}}{d \cos \theta dE} P_{e\mu}^{\text{NSI}} \right) \sigma_{\nu N}^{\text{CC}}(E) + \left(\frac{d\Phi_{\bar{\nu}_\mu}}{d \cos \theta dE} \bar{P}_{\mu\mu}^{\text{NSI}} + \frac{d\Phi_{\bar{\nu}_e}}{d \cos \theta dE} \bar{P}_{e\mu}^{\text{NSI}} \right) \sigma_{\bar{\nu} N}^{\text{CC}}(E) \right] \rho V_{\text{eff}}(E), \quad (27)$$

where Φ_{ν_α} ($\Phi_{\bar{\nu}_\alpha}$) denotes the neutrino ν_α (antineutrino $\bar{\nu}_\alpha$) fluxes, N_A is the Avogadro's number, $P_{\alpha\beta}^{\text{NSI}}$ ($\bar{P}_{\alpha\beta}^{\text{NSI}}$) stands for the neutrino (antineutrino) oscillation probabilities with NSI effects, and the effective volume of PINGU with 20 strings is parametrized as [16]

$$\rho V_{\text{eff}}(E) = 14.6 \text{ Mt} \times \left[\log_{10} \left(\frac{E}{\text{GeV}} \right) \right]^{1.8}. \quad (28)$$

Furthermore, we adopt the following simple parametrization of the deep inelastic ν - N and

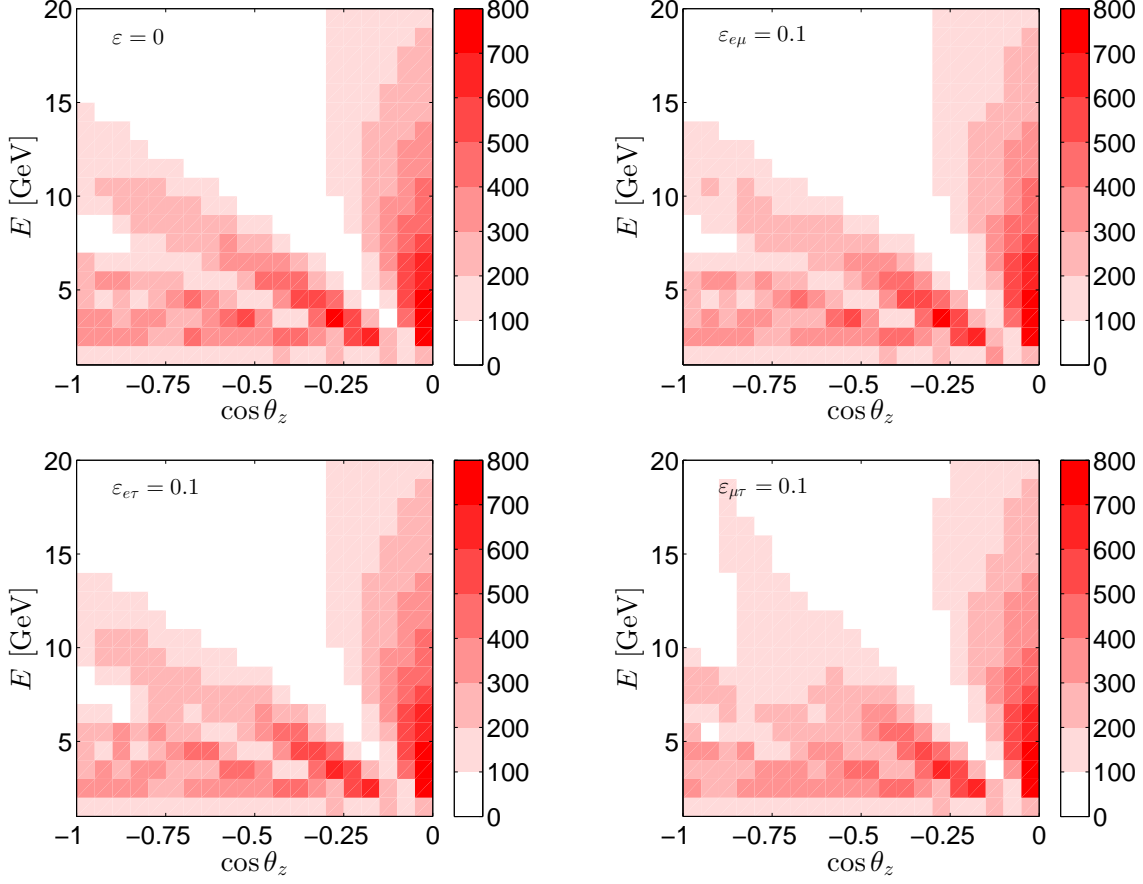


FIG. 6: The number of ν_μ -like events in the $E - \cos \theta_z$ plane, collected by the PINGU detector for one year, where the normal neutrino mass hierarchy is assumed. The upper left plot corresponds to the case of standard neutrino oscillations, i.e., all the NSI parameters are vanishing.

$\bar{\nu}$ - N scattering cross sections [16]

$$\begin{aligned}\sigma_{\nu N}^{\text{CC}}(E) &= 7.30 \times 10^{-39} \text{ cm}^2 \left(\frac{E}{\text{GeV}} \right), \\ \sigma_{\bar{\nu} N}^{\text{CC}}(E) &= 3.77 \times 10^{-39} \text{ cm}^2 \left(\frac{E}{\text{GeV}} \right).\end{aligned}\quad (29)$$

The atmospheric electron and muon neutrino fluxes are taken from Ref. [36], where the neutrino fluxes have been calculated using a hybrid method for $1 \text{ GeV} < E < 10^4 \text{ GeV}$ and tabulated in small bins of neutrino energy and zenith angle.

The event distribution in the case of standard neutrino oscillations is shown in the upper left panel of Fig. 6, where the bin widths $\Delta E = 1 \text{ GeV}$ and $\Delta \cos \theta_z = 0.05$ are used and NH is assumed. Note that the highest number of events can reach ~ 800 , which is in agreement with the estimation in Ref. [16]. It is evident that the event distribution is mainly determined by the $\nu_\mu \rightarrow \nu_\mu$ survival probability, which is given in the left panel of Fig. 3. In the presence of NSIs, the event distribution is distorted, as shown in the other plots of Fig. 6. In particular, in the case of $\varepsilon_{\mu\tau} \neq 0$, the number of events at high energy

bins is increased remarkably. This is because the $\nu_\mu \rightarrow \nu_\mu$ channel in Eq. (27) dominates the contributions to the observed ν_μ -like events, and the NSI parameter $\varepsilon_{\mu\tau}$ significantly modifies the survival probability in this region. The latter has already been pointed out in Sec. III C and illustrated in Fig. 3. Therefore, the PINGU detector has a better sensitivity to $\varepsilon_{\mu\tau}$ than $\varepsilon_{e\mu}$ and $\varepsilon_{e\tau}$. Note also that the total number of events is approximately unchanged.

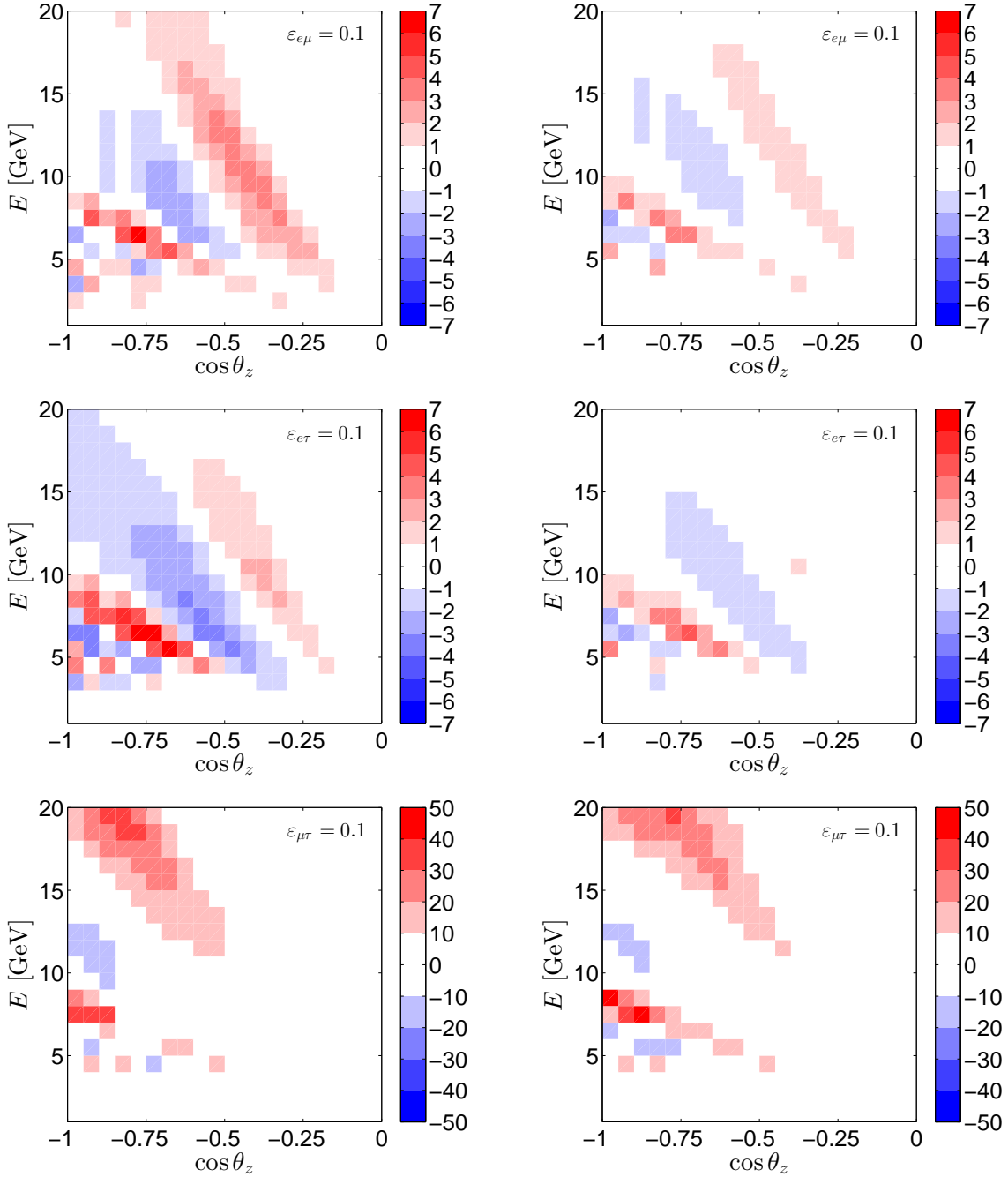


FIG. 7: The SD-NSI asymmetry $\mathcal{A} \equiv (N_\mu^{\text{SD}} - N_\mu^{\text{NSI}})/\sqrt{N_\mu^{\text{SD}}}$ of ν_μ -like events at the PINGU detector for one year, in the cases of normal neutrino mass hierarchy (left column) and inverted neutrino mass hierarchy (right column).

To quantify the significance of NSI effects, we define an SD–NSI asymmetry as the difference between the number of ν_μ -like events in the standard case (i.e., $\varepsilon_{\alpha\beta} = 0$) and that in the NSI case

$$\mathcal{A} = \frac{N_\mu^{\text{SD}} - N_\mu^{\text{NSI}}}{\sqrt{N_\mu^{\text{SD}}}} \quad (30)$$

for each bin in the $E - \cos\theta_z$ plane. In Fig. 7, we illustrate the distribution of the asymmetry \mathcal{A} for specific values of NSI parameters. In the cases of $\varepsilon_{e\mu} \neq 0$ and $\varepsilon_{e\tau} \neq 0$, the large asymmetry appears in the low energy regions $E \sim [5, 10]$ GeV, and is separated by the lines of zero asymmetry. For $\varepsilon_{e\mu} = 0.1$ or $\varepsilon_{e\tau} = 0.1$, the maximal asymmetry can be as large as $\mathcal{A} \approx 7$, which is comparable to the estimated sensitivity to the neutrino mass hierarchy [16]. As expected, in the case of a non-vanishing $\varepsilon_{\mu\tau}$, the SD–NSI asymmetry is much more stunning (e.g., $\mathcal{A} \approx 50$), indicating a great discovery potential on this NSI parameter. We have also made a comparison between NH and IH in Fig. 7, where one can observe that the asymmetry in some bins is reduced in the case of $\varepsilon_{e\mu} \neq 0$ and $\varepsilon_{e\tau} \neq 0$ for IH, while there is no significant difference in the case of $\varepsilon_{\mu\tau} \neq 0$. Therefore, the experimental sensitivity to the NSI parameters, in particular $\varepsilon_{\mu\tau}$, at the PINGU detector, is almost independent of neutrino mass hierarchy.

Note that the real sensitivity to NSI effects will actually be much lower because of systematics, the smearing effects in the reconstruction of neutrino energies and zenith angles, the uncertainties in the matter density profile and the other neutrino oscillation parameters [16]. In addition, the ν_τ interactions lead to an important background to the ν_μ events. Nevertheless, a detailed simulation on the probe of NSIs at PINGU is meaningful and will be elaborated elsewhere.

V. SUMMARY

Now we are entering a new era of precision measurements of neutrino parameters, including three leptonic mixing angles and two neutrino mass-squared differences. The ongoing and forthcoming neutrino experiments are expected to pin down neutrino mass hierarchy and to discover CP violation in the lepton sector. As the precisions of oscillation experiments gradually improve and more data are accumulated, it is promising to discover or constrain the new physics effects beyond the standard paradigm of neutrino oscillations.

One of the most widely studied scenarios is the non-standard neutrino interactions. In this paper, we have considered the NSI effects on neutrino oscillations in the Earth matter by using neutrino oscillograms. First, we derive the mapping formulas between the lepton mixing matrix in vacuum and that in matter beyond the leading order approximation. In particular, the NSI effects on the effective mixing angle $\tilde{\theta}_{13}$ have been discussed in some detail. Then, the NSI effects on the neutrino oscillograms of the Earth are investigated. The most significant difference between the standard and non-standard oscillograms appears in the $\nu_\mu \rightarrow \nu_\mu$ survival probability and in the case of $\varepsilon_{\mu\tau} \neq 0$. In addition, the CP-violating

effects in neutrino oscillations can be enhanced by the NSI effects, even if the CP-violating phases in the NSI parameters are switched off. Finally, the NSI effects in the PINGU experiment are explored. We calculate the event rate of atmospheric muon neutrinos at PINGU, and demonstrate that the future huge atmospheric neutrino experiments should have very good sensitivities to the NSI parameters, in particular $\varepsilon_{\mu\tau}$. However, a more sophisticated simulation of the NSI effects at PINGU, including the systematics and other uncertainties, is needed to make a final conclusion.

In addition to atmospheric neutrino experiments, such as PINGU, the ongoing and upcoming long-baseline neutrino oscillation experiments, which are intended for the determination of neutrino mass hierarchy and leptonic CP violation, are also sensitive to the NSI effects. In general, the future neutrino oscillation data will soon lead us either to the discovery of new effects beyond the standard oscillation scenario, or to more restrictive constraints on new physics parameters.

Acknowledgments

One of the authors (H.Z.) is indebted to Evgeny Akhmedov for useful discussions. This work was supported by the Swedish Research Council (Vetenskapsrådet), contract no. 621-2011-3985 (T.O.), the Max Planck Society through the Strategic Innovation Fund in the project MANITOP (H.Z.), and the Göran Gustafsson Foundation (S.Z.).

-
- [1] J. Beringer et al. (Particle Data Group), *Phys. Rev.* **D86**, 010001 (2012).
 - [2] T. Ohlsson, *Rep. Prog. Phys.* **76**, 044201 (2013), 1209.2710.
 - [3] M. Blennow, T. Ohlsson, and J. Skrotzki, *Phys. Lett.* **B660**, 522 (2008), hep-ph/0702059.
 - [4] M. Blennow and T. Ohlsson, *Phys. Rev.* **D78**, 093002 (2008), 0805.2301.
 - [5] N. Fornengo, M. Maltoni, R. Tomas, and J. Valle, *Phys. Rev.* **D65**, 013010 (2001), hep-ph/0108043.
 - [6] P. Huber and J. Valle, *Phys. Lett.* **B523**, 151 (2001), hep-ph/0108193.
 - [7] G. Mitsuka et al. (Super-Kamiokande Collaboration), *Phys. Rev.* **D84**, 113008 (2011), 1109.1889.
 - [8] J. Kopp, M. Lindner, T. Ota, and J. Sato, *Phys. Rev.* **D77**, 013007 (2008), 0708.0152.
 - [9] T. Ohlsson and H. Zhang, *Phys. Lett.* **B671**, 99 (2009), 0809.4835.
 - [10] R. Leitner, S. Malinsky, B. Roskovec, and H. Zhang, *JHEP* **1112**, 001 (2011), 1105.5580.
 - [11] J. Kopp, M. Lindner, and T. Ota, *Phys. Rev.* **D76**, 013001 (2007), hep-ph/0702269.
 - [12] N. Ribeiro, H. Minakata, H. Nunokawa, S. Uchinami, and R. Zukanovich-Funchal, *JHEP* **0712**, 002 (2007), 0709.1980.
 - [13] J. Kopp, T. Ota, and W. Winter, *Phys. Rev.* **D78**, 053007 (2008), 0804.2261.
 - [14] D. Meloni, T. Ohlsson, W. Winter, and H. Zhang, *JHEP* **1004**, 041 (2010), 0912.2735.
 - [15] P. Coloma, A. Donini, J. Lopez-Pavon, and H. Minakata, *JHEP* **1108**, 036 (2011), 1105.5936.

- [16] E. K. Akhmedov, S. Razzaque, and A. Y. Smirnov, *JHEP* **02**, 082 (2013), 1205.7071.
- [17] S. K. Agarwalla, T. Li, O. Mena, and S. Palomares-Ruiz (2012), 1212.2238.
- [18] D. Franco, C. Jollet, A. Kouchner, V. Kulikovskiy, A. Mereaglia, S. Perasso, T. Pradier, A. Tonazzo, and V. Van Elewycck, *JHEP* **1304**, 008 (2013), 1301.4332.
- [19] M. Ribordy and A. Y. Smirnov (2013), 1303.0758.
- [20] E. K. Akhmedov, P. Huber, M. Lindner, and T. Ohlsson, *Nucl. Phys.* **B608**, 394 (2001), hep-ph/0105029.
- [21] E. K. Akhmedov, R. Johansson, M. Lindner, T. Ohlsson, and T. Schwetz, *JHEP* **0404**, 078 (2004), hep-ph/0402175.
- [22] M. Freund, *Phys. Rev.* **D64**, 053003 (2001), hep-ph/0103300.
- [23] D. Meloni, T. Ohlsson, and H. Zhang, *JHEP* **0904**, 033 (2009), 0901.1784.
- [24] T. Kikuchi, H. Minakata, and S. Uchinami, *JHEP* **0903**, 114 (2009), 0809.3312.
- [25] A. Dziewonski and D. Anderson, *Phys. Earth Planet. Interiors* **25**, 297 (1981).
- [26] S. Davidson, C. Pena-Garay, N. Rius, and A. Santamaria, *JHEP* **0303**, 011 (2003), hep-ph/0302093.
- [27] C. Biggio, M. Blennow, and E. Fernandez-Martinez, *JHEP* **0908**, 090 (2009), 0907.0097.
- [28] P. Adamson et al. (MINOS Collaboration) (2013), 1303.5314.
- [29] M. Gonzalez-Garcia, M. Maltoni, J. Salvado, and T. Schwetz, *JHEP* **1212**, 123 (2012), 1209.3023.
- [30] M. Blennow, T. Ohlsson, and W. Winter, *Eur. Phys. J.* **C49**, 1023 (2007), hep-ph/0508175.
- [31] E. K. Akhmedov, M. Maltoni, and A. Y. Smirnov, *JHEP* **0705**, 077 (2007), hep-ph/0612285.
- [32] E. K. Akhmedov, M. Maltoni, and A. Y. Smirnov, *JHEP* **0806**, 072 (2008), 0804.1466.
- [33] W. Winter, *Phys. Lett.* **B671**, 77 (2009), 0808.3583.
- [34] T. Ohlsson, H. Zhang, and S. Zhou, *Phys. Rev.* **D87**, 053006 (2013), 1301.4333.
- [35] D. J. Koskinen, *Mod. Phys. Lett.* **A26**, 2899 (2011).
- [36] M. Honda, T. Kajita, K. Kasahara, and S. Midorikawa, *Phys. Rev.* **D52**, 4985 (1995), hep-ph/9503439.